CHAPTER 2

THEORY

My research work involved operation of the 30-kV bioengineering ion implanter (CMU3) at Chiang Mai University, designing and construction of a deceleration lens system using the ion beam optics program SIMION, installation of the deceleration lens to the CMU3 ion beam line, measurement of the decelerated ion beam energy, bombardment of naked DNA using the decelerated ion beam, and analysis of the ion-bombarded DNA form using gel electrophoresis. Therefore, in this chapter all of the relevant theories on the CMU3 ion implanter, ion beam optics, ion beam deceleration, measurement of decelerated ion beam energy and gel electrophoresis are introduced.

2.1 The 30 kV vertical bioengineering ion implanter (CMU3)

The bioengineering ion implanter CMU3 was installed about ten years ago at the Plasma and Beam Physics Research Facility, Department of Physics and Materials Science, Faculty of Science, Chiang Mai University. The ion implanter has been used almost in the biophysics field such as ion beam induced mutation of crops and gene transfer into cells. CMU3 consists of an ion source, a mass analyzer, a steering

magnet, a beam scanner, a target beam current measurement system, a small chamber, a big chamber, vacuum systems, power supplies, and support systems, as shown in Figure 2.1.

2.1.1 Ion source

Nielsen ion source (Danfysik 910)(นิติศักดิ์ ปาสาจะ, 1999) is of a hot cathode type which has electron emission from a tungsten filament to collide with atoms of gas to produce plasma. The Nielsen ion source is designed to work at high temperatures (up to 1200^{0}C) providing possibilities to be able to produce various ion species, either gaseous or solid, non-metal or metal (Yu Liangdeng, 1997). The Danfysik 910 ion source can increase the efficiency of generating plasma by a solenoid magnet due to its role in increasing the mean free path of electrons, because the electrons are influenced by the magnetic force to have the helical trajectories in order increase collision rate with atoms inside the chamber before they are captured by the anode. Ions in the ion source chamber are extracted by an electrode which has potential lower than that of the anode. An einzel lens system after the extractor focuses the ion beam which is divergent after extraction. The einzel lens consists of 3 electrodes, as shown in the Figure 2.1 of which the first and the third electrodes are at the ground potential while the second electrode is at a high voltage potential.

2.1.2 90° mass analyzing magnet

The magnet is supported and fixed vertically by a four-post steel frame work capable of being adjusted (shifted) in position both horizontally and vertically (Prakrajang, 2012). The beam line after the mass analyzing magnet is vertical in order

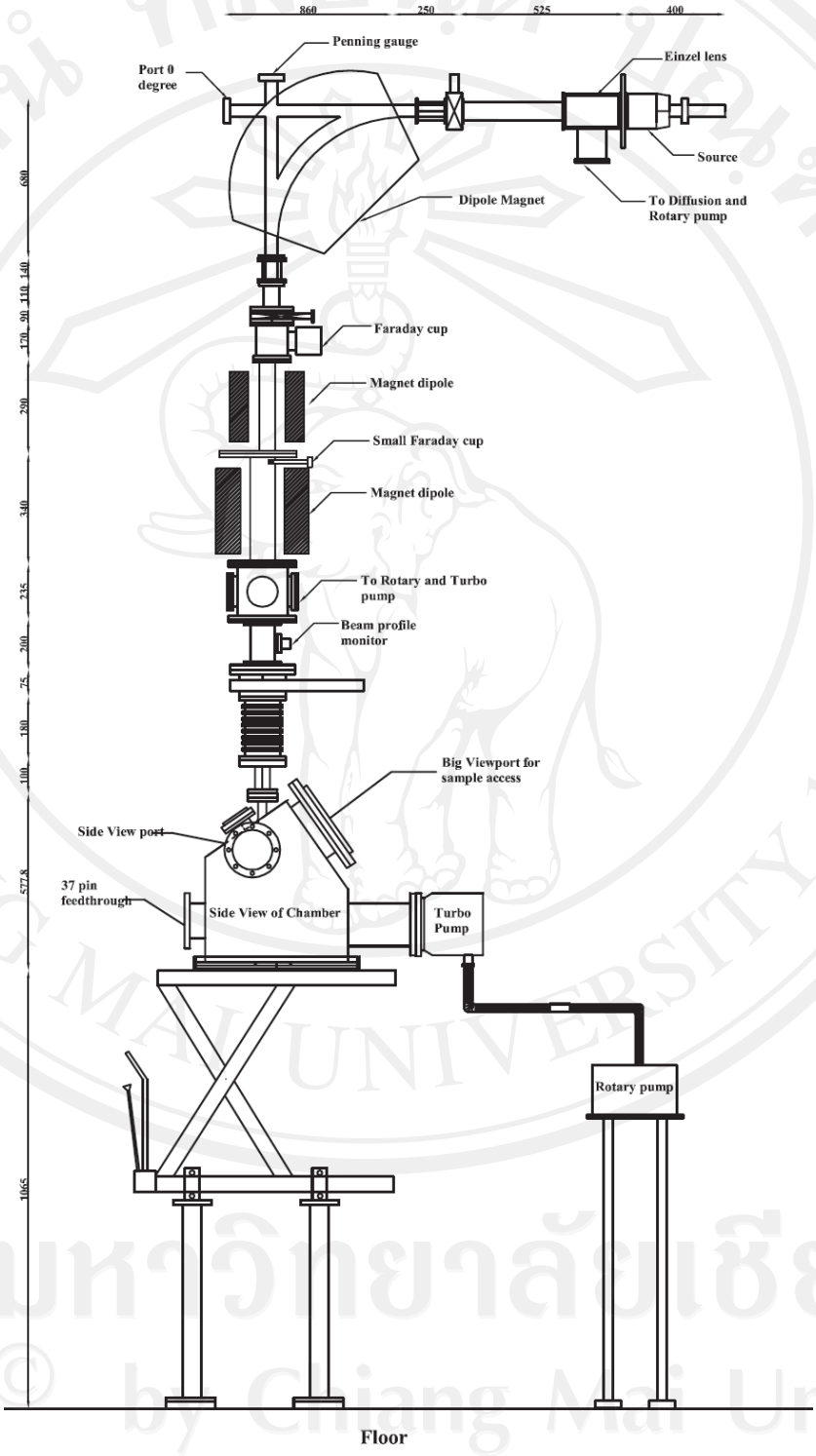

Figure 2.1. Schematic drawing of CMU3 ion beam line.

to accommodate convenient horizontal holding of biosamples which are normally very difficult to hold in vertical because of their irregular and various shapes and sizes. The dipole magnet is used to bending ion beam in horizontal plane to vertical plane, as shown in Figure 2.1. The magnetic analyzer works based on the principle of the Lorentz force. It can focus ion beam in the horizontal plane. The field at central and near central area between magnet poles is quite uniform, and the edge area is not uniform (fringe field). A fringe field plays an important role in vertical focusing. The analyzing magnet is used to select the proper ion species. Its power supply is used to supply the current up to 45 A to the magnet which can bend high current ion beam by 90° mass analyzing magnet. The magnet is cooled by chilled water (Prakrajang, 2012).

2.1.3 Double steering magnets

Two beam sweeping dipole magnets are used for separating ion beam from neutral beam and scanning ion beam for homogeneous bombardment. The first magnet bends ion beam in a small angle from the vertical direction and the second magnet bends the beam back to the vertical direction and also scans the ion beam.

2.1.4 Target chambers

The target chambers are the main components of the ion implanter. CMU3 has two target chambers. The first, a small target chamber, is installed next the steering magnet. This target chamber is used in bombardment of materials and biosamples. The size of chamber is about 20 cm in diameter and about 20 cm in height. The small chamber is designed for fast pumping to reduce the risk of biosample dehydration of staying in vacuum too long. The target chamber can be

pumped down to an order of 10^{-5} torr within 30 minutes monitoring by vacuum gauges. A Faraday cup is installed inside the chamber in order to measure the ion beam current. The movement of the sample holder is controlled by a stepping motor. Cooperation of the sample holder translation and beam scanning makes a bombarding area of 5 cm × 5 cm in maximum (Yu Liangdeng et al., 2007).

The big chamber is installed at the end of the CMU3 beam line. It is cylindrical with 45 cm in diameter and 50 cm in height for special instruments installation, for example, an *in situ* atomic force microscope (AFM), an *in situ* X-ray detecting system and the deceleration lens system.

2.2 The paraxial ray equation for axially symmetric systems

In situations where the ions move close to and with small angle to the axis, ion trajectories can be determined (Wilson and Erwer, 1973) by the paraxial ray equation for axially symmetric systems. This section will calculate ion trajectories by the paraxial approximation without space charge theory. The paraxial without space charge theory is based on the assumptions: 1) an ion is travelling close enough to the axis that the higher order terms in an expansion of the electric field can be neglected therefore the focusing of the lenses is linear with radius, and 2) the beam current is low enough so that the effect of space charge of the beam can be neglected. The ion trajectories are considered in the cylindrical coordinates. We begin with the force on the point charge q in an electromagnetic field, the Lorentz force $\boldsymbol{F}$, given by

$$\vec{F} = q(\vec{E} + \vec{v} \times \vec{B}), \tag{2.1}$$

where $\vec{E}$ is the electric field in volt per meter, $\vec{v}$ is the velocity of the moving charge in meter per second, and $\vec{B}$ is the magnetic field in tesla. The motion of particle is determined by Newton's equation

$$\frac{d\vec{P}}{dt} = \vec{F} = q(\vec{E} + \vec{v} \times \vec{B}), \tag{2.2}$$

where $\vec{P}$ is the mechanical momentum in non-relativistic mechanics, simply the product of mass and velocity. However, in relativistic mechanics the mechanical momentum is more complicated, according to the theory of special relativity, given by

$$\vec{P} = \frac{m\vec{v}}{\left(1 - v^2 / c^2\right)^{1/2}}, \text{ or } \vec{P} = \gamma m\vec{v} \ , \tag{2.3}$$

where γ is the Lorentz factor. Equation (2.2) can be expanded in cylindrical coordinates (r, θ, z). The velocity is given by $\vec{v} = \left\{\dot{r}, r\dot{\theta}, \dot{z}\right\}$ and then the equations of motion are

$$\frac{d(\gamma m\dot{r})}{dt} - \gamma m r\dot{\theta}^2 = q(E_r + r\dot{\theta}B_z - \dot{z}B_\theta), \tag{2.4}$$

$$\frac{1}{r}\frac{d\left(\gamma m r^2\dot{\theta}\right)}{dt} = q(E_\theta + r\dot{z}B_r - \dot{r}B_z), \tag{2.5}$$

$$\frac{d\left(\gamma m\dot{z}\right)}{dt} = q(E_z + \dot{r}B_\theta - r\dot{\theta}B_r). \tag{2.6}$$

The assumptions of paraxial motion are that the particle trajectories remain close to the axis [Martin Reiser, 1994], that is, r is very small compared to the radii of electrodes. Therefore, the slope of the particles trajectories remain small

$\left(r' << 1 or \dot{r} << \dot{z}\right)$, and the r' is defined by dr/dz. Furthermore, the azimuthal velocity v_θ must remain very small compared to the axial velocity $\left(r\dot{\theta} << \dot{z}\right)$. Thus, the linear approximation gives $\dot{z} = \left(v^2 - \dot{r}^2 - r^2\dot{\theta}^2\right)^{1/2} \approx v$. Due to these assumptions only first order terms in the expansion of the fields can be considered while the all term of order r^2, rr', r'^2, and higher order in the equation of motion can be dropped.

The first order electric and magnetic field terms are

$$E_z = -V', \qquad E_r = \frac{1}{2}V''r = -\frac{r}{2}\frac{\partial E_z}{\partial z}, \tag{2.7}$$

$$B_r = -\frac{1}{2}B'r, \qquad B_z = B. \tag{2.8}$$

Note that $E_\theta = 0, B_\theta = 0,$ which follow from $\vec{\nabla}\times\vec{E} = 0$ and $\vec{\nabla}\times\vec{B} = 0$ with $\partial/\partial\theta = 0$. $V = V(z)$ and $B = B(z)$ are the electrostatic potential and magnetic field on the z-axis $(r = 0)$, respectively.

If we substitute the electric and magnetic field equations (2.7) and (2.8) into equations (2.4) to (2.6), we can obtain the radial, azimuthal, and axial equations of motion as the following,

$$m\frac{d(\gamma\dot{r})}{dt} - \gamma m r\dot{\theta}^2 = \frac{qr}{2}V'' + qr\dot{\theta}B, \tag{2.9}$$

$$\gamma m r^2\dot{\theta} = -\frac{q}{2\pi}\psi + p_\theta = -\frac{q}{2}Br^2 + p_\theta, \tag{2.10}$$

$$m\frac{d\left(\gamma \dot{z}\right)}{dt} = -qV' + \frac{q}{2}r^2\dot{\theta}B'. \tag{2.11}$$

Here ψ $\left[\psi = \int \vec{B}\cdot d\vec{S} = \int \left(\vec{\nabla}\times\vec{A}\right)\cdot d\vec{S} = \oint \vec{A}\cdot d\vec{l} = 2r\pi A_\theta\right]$ is the magnetic flux enclosed by the particle trajectory, and p_θ $\left[p_\theta = \gamma m r^2\dot{\theta} + qrA_\theta = rP_\theta + qrA_\theta = const\right]$ is the canonical angular momentum, respectively. Since in the paraxial approximation $\dot{z} \approx v = \beta c (v_\theta = r\dot{\theta} << v)$, we can neglect the term $qr^2\dot{\theta}B'/2$ on the right hand side of equation (2.11). The left hand side term in the equation (2.11) can be changed into differentiation with respect to the z-coordinate as following,

$$\frac{d\left(\gamma \dot{z}\right)}{dt} = \frac{dz}{dt}\frac{d}{dz}\left(\gamma \dot{z}\right) = v\frac{d}{dz}(\gamma v) = \gamma' v^2 + \gamma v' v = c^2\left(\gamma'\beta^2 + \gamma\beta'\beta\right),$$

or, with $\beta'\beta = \gamma'/\gamma^3$,

$$\frac{d\left(\gamma \dot{z}\right)}{dt} = c^2\left(\beta^2 + \gamma^{-2}\right)\gamma' = c^2\gamma'.$$

Thus, equation (2.11) may be written as

$$mc^2\gamma' = -qV'. \tag{2.12}$$

From equation (2.10) we obtain the angular velocity of the particles

$$\dot{\theta} = -\frac{qB}{2\gamma m} + \frac{p_\theta}{\gamma m r^2},$$

or

$$\theta' = \frac{\dot{\theta}}{\beta c} = -\frac{qB}{2\gamma m\beta c} + \frac{p_\theta}{\gamma m\beta c r^2}. \tag{2.13}$$

Substitution equation (2.13) into equation (2.9) obtains for the radial motion

$$\frac{d(\gamma \dot{r})}{dt} = \frac{qrV''}{2m} + \frac{r\dot{\theta}}{m}\left(m\gamma\dot{\theta} + qB\right)$$

$$\frac{d(\gamma \dot{r})}{dt} = \frac{qrV''}{2m} + \frac{r}{m}\left(-\frac{qB}{2\gamma m} + \frac{p_\theta}{\gamma m r^2}\right)\left(\frac{qB}{2} + \frac{p_\theta}{r^2}\right),$$

or
$$\frac{d(\gamma \dot{r})}{dt} = \frac{qrV''}{2m} - \frac{r}{4}\left(-\frac{qB}{m}\right)^2\frac{1}{\gamma} + \frac{p_\theta^2}{\gamma m^2 r^3}. \tag{2.14}$$

Now we consider

$$\dot{\gamma} = \gamma'\dot{z} = \gamma'\beta c, \tag{2.15}$$

$$\dot{r} = r'\dot{z} = r'\beta c, \tag{2.16}$$

$$\ddot{r} = \beta c\frac{d}{dz}(r'\beta c) = r''\beta^2 c^2 + r'\beta'\beta c^2. \tag{2.17}$$

By using equation (2.15) to equation (2.17) and the relation $\beta'\beta = \gamma'/\gamma^3$, the left hand side of equation (2.14) may be written as

$$\frac{d(\gamma \dot{r})}{dt} = c^2\left(\gamma\beta^2 r'' + \gamma' r'\right). \tag{2.18}$$

From equation (2.12), we have

$$qV'' = -mc^2\gamma''. \tag{2.19}$$

Substitution of equations (2.18) and (2.19) into equation (2.14) yields

$$r'' + \frac{\gamma'}{\gamma\beta^2}r' + \frac{\gamma''}{2\gamma\beta^2}r + \left(\frac{qB}{2mc\beta\gamma}\right)^2 r - \frac{p_\theta^2}{m^2c^2\gamma^2\beta^2 r^3} = 0. \tag{2.20}$$

This is the relativistically corrected paraxial ray equation that defines the radial motion of the particles near the z-axis where the non linear force terms are neglected.

The azimuthal position of the particles as a function of distance z can be determined by equation (2.13).

The meaning of each term of equation (2.20) is as follows. The first term, r'' represents the change the slope of the particle trajectory. The second term contains the effect of the axial electric field (acceleration or deceleration). The third term concerns the radial electric field (focusing or defocusing). The fourth term represents the magnetic force. The last term adds a centrifugal potential or an effective repulsive core when the canonical angular momentum is different from zero, and in this case the particle never crosses the axis.

In the non-relativistic limit, we can make the substitutions

$$\gamma \approx 1, \qquad \beta^2 = \frac{v^2}{c^2} \approx -\frac{2qV}{mc^2}, \tag{2.21}$$

$$\gamma' \approx -\frac{qV'}{mc^2}, \quad \frac{\gamma'}{\beta^2} \approx \frac{V'}{2V}, \tag{2.22}$$

$$\gamma'' \approx -\frac{qV''}{mc^2}, \quad \frac{\gamma''}{\beta^2} \approx \frac{V''}{2V}. \tag{2.23}$$

By these approximations, the equation (2.20) can be written in the non-relativistic paraxial ray equation

$$r'' + \frac{V'r'}{2V} + \frac{V''r}{4V} + \frac{q^2B^2r}{8mqV} - \frac{p_\theta^2}{2mqV}\frac{1}{r^3} = 0. \tag{2.24}$$

For the angle θ, the non-relativistic approximation from equation (2.13) (the initial condition $\theta = \theta_0$ and $z = z_0$) gives

$$\theta = \theta_0 - \int_{z_0}^{z}\left[\left(\frac{q^2B^2}{8mqV}\right)^{1/2} - \frac{p_\theta}{(2mqV)^{1/2}r^2}\right]dz. \tag{2.25}$$

2.3 Beam optics

Section 2.2 considers the ion trajectories by paraxial without space charge approximation, and finally obtains equation (2.20). However, my research has been focused in ultra-low ion beam energy and concentrated on an electric field only, and thus the fourth term in the equation vanishes. As the initial angular velocity is zero, the last term in the non-relativistic approximation of the paraxial ray equation vanishes. Then equation (2.24) becomes

$$r'' + \frac{V'r'}{2V} + \frac{V''r}{4V} = 0 . \qquad (2.26)$$

The paraxial ray equation (2.26) can be integrated and the equation essentially relates the change in transverse momenta between the two planes. A direct integration of equation (2.26) is very difficult. However there is a transformation method for calculation of the ion trajectories. Ion beam optics characteristics of each element can be expressed by transformation which relates the radius and slope of ion trajectories at the input and output planes. This transformation forms a matrix which conveniently multiplies with the matrix of each optical element.

For example, a double-aperture lens is shown in Figure 2.2. The ion beam trajectories are calculated by the transformation matrix method. The matrices of the double-aperture lens consist of the matrix of aperture lens (M_{12} and M_{34}) and the matrix of constant field region between potentials V_1 and V_2 (M_{23}). Then the trajectories of ion beam are

$$\begin{pmatrix} r_4 \\ \sqrt{V_4}r_4' \end{pmatrix}_i = M_{34} \cdot M_{23} \cdot M_{12} \begin{pmatrix} r_1 \\ \sqrt{V_1}r_1' \end{pmatrix}_o = M_{DL} \begin{pmatrix} r_1 \\ \sqrt{V_1}r_1' \end{pmatrix}_o = \begin{pmatrix} a_{11} & a_{12} \\ a_{21} & a_{22} \end{pmatrix} \begin{pmatrix} r_1 \\ \sqrt{V_1}r_1' \end{pmatrix}_o , \quad (2.27)$$

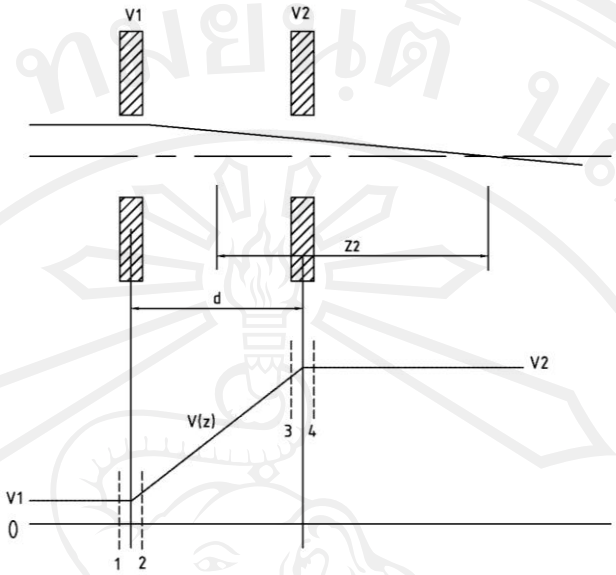

Figure 2.2. Schematic diagram of a double-aperture lens (Wilson and Erwer, 1973).

where r and r' represent the transverse position and the slope in the r plane, respectively. Subscription i and o represent the position and the slope at the image (ion beam exit) and the object (ion beam entrance) plane, respectively. Details of matrices will be shown later.

The focal length (f) of lens system is

$$-\frac{1}{f} = a_{21}. \tag{2.28}$$

If a focal length is positive, it is converging and vice versa. The Lagrange invariant imposes the condition that the determinant of the matrix is unity,

$$a_{11} \cdot a_{22} - a_{12} \cdot a_{21} = 1. \tag{2.29}$$

2.3.1 Transformation matrix of the drift space

Ion beams in a field free drift space of length L at potential V between input and output reference planes (Figure 2.3) will travel in straight lines. The transverse velocity is constant and change in transverse position is just equal to slope of the input trajectory multiplied by the drift length. As shown in Figure 2.3,

$$r_2 = r_1 + Lr_1' \tag{2.30}$$

$$r_2' = r_1'. \tag{2.31}$$

It can be written in a transformation matrix format:

$$\begin{pmatrix} r_2 \\ \sqrt{V} r_2' \end{pmatrix}_i = \begin{pmatrix} 1 & \frac{L}{\sqrt{V}} \\ 0 & 1 \end{pmatrix} \begin{pmatrix} r_1 \\ \sqrt{V} r_1' \end{pmatrix}_o = M_D \begin{pmatrix} r_1 \\ \sqrt{V} r_1' \end{pmatrix}_o, \tag{2.32}$$

where M_D is the drift space transformation matrix. The potential in the drift space is constant, thus $V = V_1 = V_2$.

2.3.2 Transformation matrix of the uniform field (Liebl, 2008)

The trajectory and slope of ion beam after passing through a uniform electric field when considering the paraxial case (Figure 2.4) can be determined by using the transformation matrix. The transformation matrix of the uniform field is

$$\begin{pmatrix} r_2 \\ \sqrt{V_2} r_2' \end{pmatrix}_i = \begin{pmatrix} 1 & \frac{2L}{\sqrt{V_1} + \sqrt{V_2}} \\ 0 & 1 \end{pmatrix} \begin{pmatrix} r_1 \\ r_1' \end{pmatrix}_o = M_F \begin{pmatrix} r_1 \\ \sqrt{V_1} r_1' \end{pmatrix}_o, \tag{2.33}$$

where M_F is the uniform field transformation matrix. For the ion beam, $V_1 > V_2$ is an acceleration case, while $V_1 < V_2$ is a deceleration case and $V_1 = V_2$ is a drift space case.

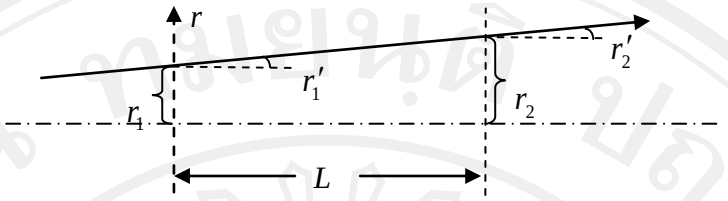

Figure 2.3. Drift space without deflection (Liebl, 2008).

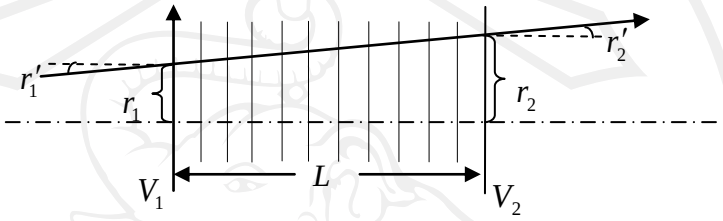

Figure 2.4. Paraxial case of acceleration of charged particle through a uniform field (Liebl, 2008). For clarity, the length of r_1 and r_2 are enlarged.

2.3.3 Transformation matrix of double-aperture lens (Wilson and Erwer, 1973)

From Figure 2.2, a double-aperture lens is composed of two apertures and there is no electric field before the first electrode. The focal length of the first aperture is given by

$$\frac{1}{f_1} = \frac{1}{4L}\left(\frac{V_2 - V_1}{\sqrt{V_1}}\right). \tag{2.34}$$

And the focal length of the second aperture is given by

$$\frac{1}{f_2} = \frac{1}{4L}\left(\frac{V_1 - V_{21}}{\sqrt{V_2}}\right). \tag{2.35}$$

The matrices of double aperture lenses are

$$M_{12} = \begin{pmatrix} 1 & 0 \\ \dfrac{V_1 - V_2}{4L\sqrt{V_1}} & 1 \end{pmatrix} \tag{2.36}$$

and

$$M_{34} = \begin{pmatrix} 1 & 0 \\ \dfrac{V_2 - V_1}{4L\sqrt{V_2}} & 1 \end{pmatrix}. \tag{2.37}$$

By using equations (2.33), (2.36) and (2.37) to equation (2.27), it is then

$$\begin{pmatrix} r_4 \\ \sqrt{V_4}\, r_4' \end{pmatrix}_i = \begin{pmatrix} \dfrac{3\sqrt{V_1} - \sqrt{V_2}}{2\sqrt{V_1}} & \dfrac{2L}{\sqrt{V_1} + \sqrt{V_2}} \\ \left[\dfrac{3(V_2 - V_1)}{8d} \cdot \dfrac{\sqrt{V_1} - \sqrt{V_2}}{\sqrt{V_1 V_2}}\right] & \dfrac{3\sqrt{V_2} - \sqrt{V_1}}{2\sqrt{V_2}} \end{pmatrix} \begin{pmatrix} r_1 \\ \sqrt{V_1}\, r_1' \end{pmatrix}_o = M_{DL} \begin{pmatrix} r_1 \\ \sqrt{V_1}\, r_1' \end{pmatrix}_o, \tag{2.38}$$

where M_{DL} is the double-aperture lens transformation matrix. This matrix can be used as an approximation to that representing an accelerating or decelerating gap between plates or cylinders. It will form a more accurate representation as the ratio of the gap length (L) to the aperture diameter becomes larger.

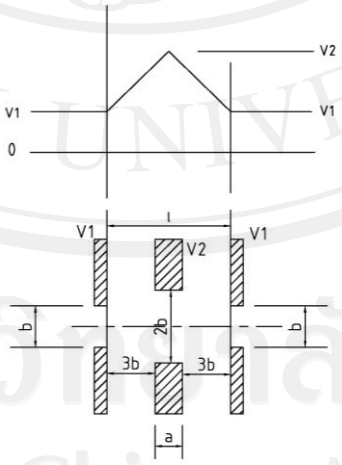

Figure 2.5. Schematic diagram of the Einzel lens arrangement and potential variation (above the lens) (Wilson and Erwer, 1973).

2.3.4 Transformation matrix of einzel lens (Wilson and Erwer, 1973)

An einzel lens is composed of 3 electrodes, in which the first and the third electrodes have the same potentials (Figure 2.5). The einzel lens is used to focus ion beam trajectory without changing the energy. The einzel lens initially decelerates $(V_2 > V_1)$ ions, yielding ion trajectories closer to the axis (than the case $V_1 > V_2$) and thereby losing spherical aberration. The transformation matrix of the Einzel lens is

beam trajectory without changing the energy. The einzel lens initially decelerates $(V_2 > V_1)$ ions, yielding ion trajectories closer to the axis (than the case $V_1 > V_2$) and thereby losing spherical aberration. The transformation matrix of the Einzel lens is

$$M = \begin{vmatrix} \dfrac{16\sqrt{V_1V_2} - 6V_1 - 6V_2}{4\sqrt{V_1V_2}} & \dfrac{2d}{\sqrt{V_1}+\sqrt{V_2}}\dfrac{\sqrt[3]{V_2}-\sqrt{V_1}}{\sqrt{V_2}} \\ \dfrac{3}{8}\dfrac{(V_1-V_2)}{d}\left(\dfrac{\sqrt{V_2}-\sqrt{V_1}}{\sqrt{V_1V_2}}\right)\left(\dfrac{3\sqrt{V_1}-\sqrt{V_2}}{\sqrt{V_1}}\right) & \dfrac{16\sqrt{V_1V_2} - 6V_1 - 6V_2}{4\sqrt{V_1V_2}} \end{vmatrix}. \quad (2.39)$$

From the transformation matrix of Einzel lens, one can find that a positive focal length $(V_2 > V_1)$ means that this lens has the property of focusing ion beam, while if all electrodes have the same potential $(V_1 = V_2)$, the focal length equals to infinity.

2.4 Aberrations in the ion optical elements

The size and shape of a focused ion beam can be strongly influenced by imperfections in the several ion optical elements which make up the beam transport system (Wilson and Erwer, 1973). The important four types of aberrations will be described in the following. The spherical and chromatic aberrations are shown in

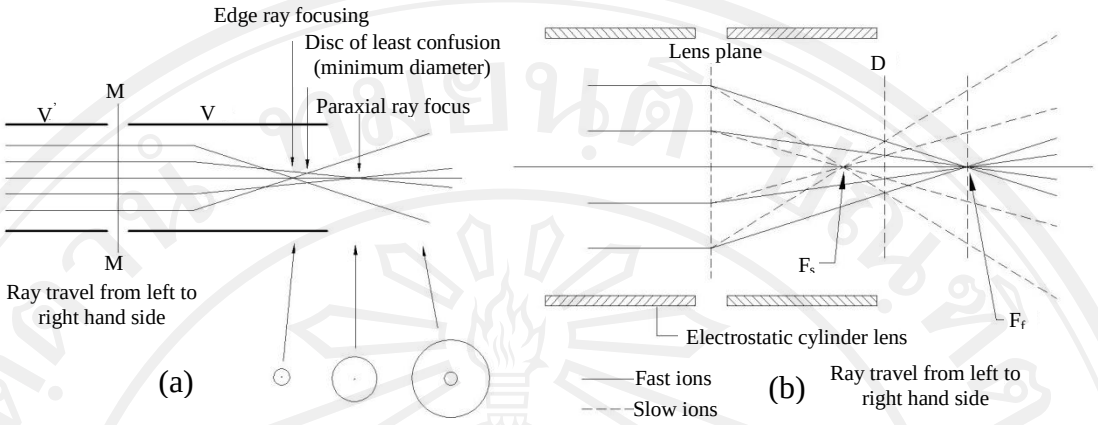

Figure 2.6. Schematic diagrams of typical trajectories exhibiting (a) spherical aberration and (b) chromatic aberration (Wilson and Erwer, 1973).

Figure 2.6.

From Figure 2.6 (a), aberrations will result in a minimum beam diameter, which is called the disk of least confusion. This minimum diameter results from the crossing of several ion trajectories passing through the lens that does not come to a focus at the same axial position, in contrast with the beam minimum due to space charge repulsion (Orloff, 2009).

2.4.1 Spherical aberration

This defect is caused by focusing fields that are invariably stronger near that the electrodes that produce them, usually result of the focal position closer to the lens than the paraxial focal position, as shown in Figure 2.6 (a). For the disk of the least confusion, radius δ_s is given by

$$\delta_s = (1/4)C_s\alpha_i^3, \tag{2.40}$$

where C_s is the spherical aberration constant, usually relates to the paraxial focal length f by $C_s = K_s f$, K_s a constant dependent on the lens geometry, and α_i is the convergence haft-angle at the image side of the lens. α_i can be related to the equivalent angle on the object side α_o by the Lagrange-Helmholz relation (Grivet, 1965)

$$\sqrt{V_0} h_0 \alpha_0 = \sqrt{V_i} h_i \alpha_i , \tag{2.41}$$

where V_0 and V_i are the potentials, h_0 and h_i are the distances of the ray from axis on object and image sides of the lens, respectively. The spherical aberration is impossibly eliminated from beam, therefore it is of the great importance to design the element with minimum spherical aberration constant (C_s).

2.4.2 Chromatic aberration or the effect of momentum dispersion

The chromatic aberration in a lens refers to the sensitivity of the focal properties to the velocity with which the particles enter the lens. A higher velocity particle will come to a focus farther from the lens than a particle with lower entrance velocity. For the disk of the least confusion in chromatic aberration case [Figure 2.6(b)], the radius (δ_c) is given by

$$\delta_c = C_c \alpha_i \frac{\Delta V}{V_0} , \tag{2.42}$$

where C_c is the chromatic aberration constant, frequently expressed as $C_c = K_c f$. ΔV and V_0 represent the energy spread and the mean energy of the incoming ions, respectively. The chromatic aberration depends on the parameters of the lens characteristics, the incident ion energies, and electronic aberration. Since the lens

characteristics depend on the applied voltage, therefore the chromatic aberration will occur if the voltages vary because of power supply ripple or drift.

2.4.3 Ellipticity astigmatism

This aberration can occur if the apertures of electrostatic optical elements are not circular, or are displaced or tilted with respect to the optical axis. In these cases the elliptical shape of the resulting electric field will cause an aberration called ellipticity astigmatism. The disk radius of confusion is given by

$$\delta_e = C_e \alpha_i . \tag{2.43}$$

For a noncircular aperture, C_e is the ellipticity constant. Grivet gives equations relating the mechanical displacement or tilt of the principle aperture of a lens to the ellipticity constant. If this aperture is displaced off center by Δe with respect to the optical axis, then the ellipticity constant is

$$C_e = C_s \left(\frac{\Delta e}{f} \right)^2 \tag{2.44}$$

where C_s is the spherical aberration coefficient. If a circular lens is tilted at an angle β with respect to the optical axis, the ellipticity constant is given by

$$C_e = C_s \beta^2 \tag{2.45}$$

This aberration can be decreased by serious concerns in the designing and construction of ion optical elements since the astigmatism results from mechanical type error. The astigmatism can be corrected by the use of a stigmator which, in its simplest form, is an n-pole element of opposite electric fields arranged around the beam (Wilson and Erwer, 1973).

2.4.4 Diffraction

In passing through a limited aperture, a beam will be diffracted to form a spot of radius

$$\delta_d \cong \frac{0.6\lambda}{\alpha}, \tag{2.46}$$

where $\lambda=0.286/(V_0M)^{1/2}$ Å for ions V_0=potential(V), M=atomic mass. This effect will be a limitation only in very high resolution devices and is not usually of practical importance.

2.4.5 Total aberration

If the several aberrations discussed above are independent, the observed minimum beam radius at the focused spot can be represented by

$$\delta_{observed} = \sqrt{\delta_c^2 + \delta_e^2 + \delta_s^2}\ . \tag{2.47}$$

The radii of the disks of confusion are added as the rms sum. Practical beam transport systems will be made up of several ion-optical elements, each contributing distortion to the beam. It is of interest to be able to determine the total aberration resulting from two lenses in series. The effect of additional lenses can obviously be determined by repeating use of the relation for two lenses (Liebmann, 1949).

2.5 Ion beam energy deceleration

A retarding field is used for decelerating ion beam since the force direction of the retarding field is opposite to the incident direction of ion beam, as shown in Figure 2.7. In this section, the methods for calculating the ion beam energy deceleration are described. There are two methods, the first considering the energy

conservation principle in the mechanic theory and the second considering principles in the electrostatic theory. The second method can be separated in two cases which are ions motion between electrode plates without space charge and with space charge effects.

In Figure 2.7, two infinite parallel conducting plates are considered. The first plate is at $x = 0$ with potential $\phi = V_1$ and the second plate is at $x = d$ with potential $\phi = V_2$. Such a configuration is known as a planar diode. The primary ion beam enters the planar diode field from the left at the entrance aperture and the decelerated ion beam leaves the field from the exit at the right.

2.5.1 Ion beam energy deceleration by mechanical theory

The energy conservation principle states that energy cannot be created or destroyed but it can be changed from one form to another. Thus, in an isolated or closed system the sum of all forms of energy remains constant. In the case of using the retarding field to decelerate ions, the energy conservation is

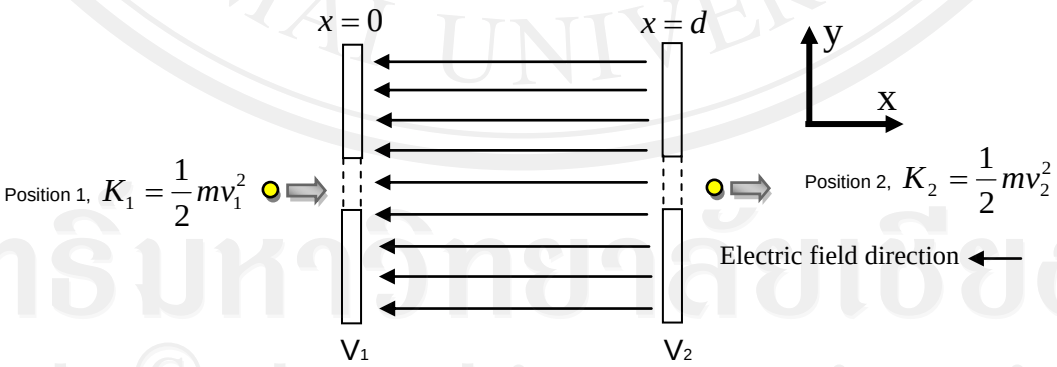

Figure 2.7. A schematic diagram of ion beam deceleration to lower the ion energy by a retarding field (Liebl, 2008).

$$E_{total} = E_{total,1} = E_{total,2} = K_1 + P_1 = K_2 + P_2, \quad (2.48)$$

where E_{total} is the total energy, E_1 is the ion energy at the entrance position, position 1, where an ion beam has the kinetic energy gained from the ion source extraction/acceleration only, E_2 is the ion energy at the exit position, position 2, where the ion beam passes the retarding field and has the kinetic energy but affected by the potential energy, assuming the electrostatic field between the plates uniform, K is the kinetic energy and P is the potential energy. From Figure 2.7, following the energy conservation principle, one has

$$\frac{1}{2}mv_1^2 = \frac{1}{2}mv_2^2 - q(V_1 - V_2) \rightarrow \frac{1}{2}mv_2^2 = \frac{1}{2}mv_1^2 + q(V_1 - V_2) \ , \quad (2.49)$$

where v_1 is the ion velocity at position 1, v_2 is the ion velocity at position 2, q is proton charge, V_1 is the voltage of plate 1 and V_2 is the voltage of plate 2.

The total ion energy at position 1 has only the kinetic energy since the ion beam is extracted/accelerated from the ion source and the total energy at position 2 has the kinetic energy and affected by the potential energy which is given by the retarding field between two electrode plates. For a retarding field, V_1 is lower than V_2 ; if $V_1 = V_2$, that is a free space. For example, an ion beam extracted from the ion source has energy of 15 keV at position 1; after it passes through the retarding field which has V_1 and V_2 to be 0 and 14.5 kV, respectively, thus from energy conservation principle one can know that the ion beam energy at position 2 is 0.5 keV (assuming singly charged ion).

2.5.2 Ion beam energy deceleration by electrostatic theory

2.5.2.1 Analytic ion beam energy deceleration without space charge

For convenience in analyis, the parameters are defined as following: the first plate at $x = 0$ with potential $\phi = 0$ and the second plate at $x = d$ with potential $\phi = V$, respectively. The static electric field between the two plates is given by $\vec{E} = -\vec{\nabla}\phi$ and the potential $\phi(x)$ can be calculated from Laplace's equation (without space charge case, $\rho = 0$)

$$\vec{\nabla}^2\phi = \frac{d^2\phi}{d^2x} = 0, \tag{2.50}$$

with the solution

$$\phi(x) = -\frac{V}{d}x, \tag{2.51}$$

and

$$E_x = E = -\frac{d\phi}{dx} = \frac{V_0}{d}, \tag{2.52}$$

the electric field is uniform between plates.

The non-relativistic equations of motion in Newton's form in the x-direction are (in Figure 2.7 it can seen that the electrostatic field direction is opposite to the ion velocity direction),

$$m\ddot{x} = -qE, \tag{2.53}$$

$$\dot{x} = -\frac{q}{m}Et + \dot{x}_0, \tag{2.54}$$

$$x = -\frac{qE}{m}\frac{t^2}{2} + \dot{x}_0 t, \tag{2.55}$$

and in the y-direction,

$$m\ddot{y} = 0, \tag{2.56}$$

$$\dot{y} = \dot{y}_0, \tag{2.57}$$

$$y = \dot{y}_0 t. \tag{2.58}$$

Substituting $t = y/\dot{y}_0$ from equation (2.58) into equation (2.55) gives the trajectory equation

$$x = -\frac{1}{2}\frac{qE}{m}\frac{y^2}{\dot{y}_0^2} + \frac{\dot{x}_0}{\dot{y}_0}y, \tag{2.59}$$

which is a parabola.

The kinetic energy loss is $\Delta T = T - T_0 = \frac{m}{2}\left(\dot{x}^2 - \dot{x}_0^2\right)$. From equation (2.54),

$$\dot{x}^2 - \dot{x}_0^2 = \left(-\frac{qEt}{m}\right)^2 - 2\frac{qEt}{m}\dot{x}_0. \tag{2.60}$$

Substituting $\dot{x}_0 = \frac{x}{t} + \frac{qEt}{2m}$ from equation (2.55) into equation (2.60) gives the kinetic energy loss,

$$\Delta T = T - T_0 = \frac{m}{2}\left(\dot{x}^2 - \dot{x}_0^2\right) = -qEx. \tag{2.61}$$

In the case without space charge, the kinetic energy loss $qV_0\frac{x}{d}$ and ΔT loss qV_0, when ion arrives the second plate, from the analytic ion energy deceleration in the energy conservation principle and the electrostatic without space charge theory have the results corresponding to each other.

2.5.2.2 Analytic ion beam energy deceleration with space charge

Let us now include the effect of the space charge of the ion current in the planar diode on the potential distribution and ion motion. To simplify analysis, all ions are launched with initial velocity zero from the first plate. The electrostatic potential is determined from the space charge density ρ via Poisson's equation (Reiser, 1994). The relationship between ρ, the current density $\vec{J}$, and the ion velocity follows from the continuity equation. To solve the effect, the three equations are used as the following,

$$\vec{\nabla}^2\phi = \frac{d^2\phi}{dx^2} = -\frac{\rho}{\varepsilon_0} \qquad \text{(Poisson's equation),} \tag{2.62}$$

$$J_x = \rho \dot{x} = const \qquad \text{(Continuity equation),} \tag{2.63}$$

$$\frac{1}{2} m \dot{x}^2 = q\phi(x) \qquad \text{(equation of motion).} \tag{2.64}$$

Substituting $\dot{x} = \left[2q\phi(x)/m\right]^{1/2}$ from equation (2.64) into equation (2.63) and $\rho = J_x / \dot{x}$ from equation (2.63) into equation (2.62) yields

$$\frac{d^2\phi}{dx^2} = \frac{J}{\varepsilon_0 (2q/m)^{1/2}} \frac{1}{\phi^{1/2}}, \tag{2.65}$$

where the current density $J = -J_x$ is defined as a positive quantity. After multiplication of both sides of equation (2.65) with $\frac{d\phi}{dx}$, we can integrate and obtain

$$\left(\frac{d\phi}{dx}\right)^2 = \frac{4J}{\varepsilon_0 (2q/m)^{1/2}} \phi^{1/2} + C. \tag{2.66}$$

Now $\phi = 0$ at $x = 0$, and if we consider a special case where $d\phi/dx = 0$ at $x = 0$, we obtain $C = 0$. A second integration yields

$$\frac{4}{3}\phi^{3/4} = 2\left(\frac{J}{\varepsilon_0}\right)^{1/2}\left(\frac{2q}{m}\right)^{-1/4} x. \tag{2.67}$$

Using boundary condition, $\phi = V_0$ at $x = d$ gives the equation

$$J = \frac{4}{9}\varepsilon_0\left(\frac{2q}{m}\right)^{1/2}\frac{V_0^{3/2}}{d^2}, \tag{2.68}$$

which is known as the Child's law or the Child-Langmuir law. Substitution of Equation (2.68) into equation (2.67) and rearrangement of the variables yield

$$\phi(x) = -V_0\left(\frac{x}{d}\right)^{4/3}. \tag{2.69}$$

The kinetic energy loss in this case, from equation (2.61) $(\Delta T = -qEx)$ and equation (2.52) $\left(E_x = E = -\frac{d\phi}{dx}\right)$, is

$$\Delta T = -qEx = -q\left[\frac{4V_0}{3d}\left(\frac{x}{d}\right)^{1/3}\right]x \tag{2.70}$$

In the case with space charge, the kinetic energy loss $q\left[\frac{4V_0}{3d}\left(\frac{x}{d}\right)^{1/3}\right]x$ and ΔT loss $\frac{4}{3}qV_0$, when ion arrives the second plate, can be seen 4/3 times that (eq. 2.61) without space charge effect.

2.6 Measurement of decelerated low-energy ion beam by using a deflecting electrostatic field

The deceleration lens system is designed and constructed for reducing ion beam energy from keV to 10-100 eV. To verify the deceleration effect, measurement of ion beam energy must be done. There have been some methods of the measurement of the decelerate ion beam energy. I used a simpler, cheaper and reliable method, that is, using a deflecting electrostatic field to bend the ion beam and the beam bending distance being related to the ion energy. The method is described in details in this section.

The basic idea is to use a uniform electrostatic field to deflect the beam, as shown in Figure 2.8, and the deflection distance depends on the ion energy.

When an ion beam passes an electrostatic field whose direction is perpendicular to the ion beam travelling direction, its ion beam is bent in a quadratic path. After exiting from the end of the electrostatic field the ion beam trajectory is in a straight line. If the electrode plates are too short, the electrostatic field may not be uniform and have an edge effect. Thus, to reduce the edge effect, the electrode plates must not be too short. The electrostatic force on an ion passing through the field is

$$F = eU / d , \tag{2.71}$$

where e is the unit charge, assuming that the ion is a singly charge. This force deflects the ion's trajectory and also accelerates the ion in the perpendicular direction to a final velocity v_h after the ion leaves the field, but does not change the ion velocity v_0 along the incident direction.

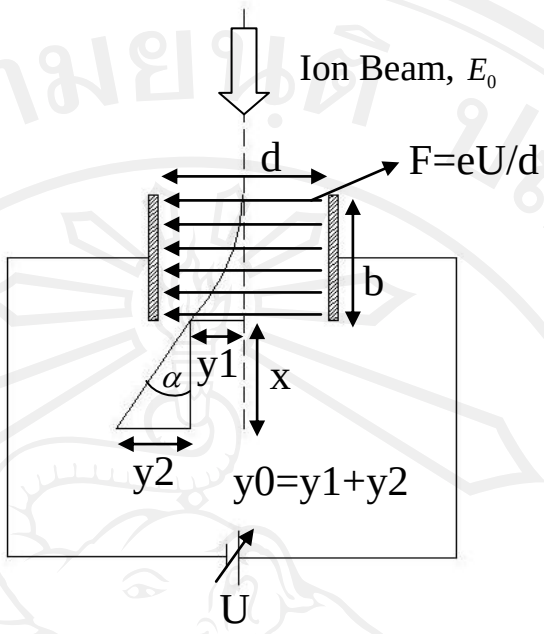

Figure 2.8. A schematic diagram of the method to measure the ion beam energy in this work.

2.6.1 The first part: considering an ion passing through an electric field

From the Newton's second law and eq. (2.71), we have

$$\vec{F} = m\vec{a} \Rightarrow \frac{eU}{d} = ma_y \,. \tag{2.72}$$

The electric field has the effect on the moving ion in the direction (y-axis) perpendicular to the ion moving direction and the time duration of the ion passing the field is

$$t_1 = \frac{b}{v_0} \,. \tag{2.73}$$

The equation of ion's trajectory is then

$$y_1 = u_{0y}t_1 + \frac{1}{2}a_y t_1^2 \,, \tag{2.74}$$

where y_1 is the deflecting distance, u_{0y} is initial velocity in perpendicular direction which equals to zero. From eq. (2.72) and eq. (2.73), the equation of ion's trajectory, i.e. eq. (2.74), becomes

$$y_1 = \frac{1}{2}\left[\frac{eU}{md}\right]\left[\frac{b}{v_0}\right]^2 = \frac{1}{2}\left[\frac{eUb^2}{d}\right]\left[\frac{1}{(1/2)mv_0^2}\right]\bullet\frac{1}{2} = \frac{1}{4}\frac{eUb^2}{E_0 d}, \qquad (2.75)$$

where U is in volt and E_0 is the original ion energy in eV.

2.6.2 The second part: considering the ion's trajectory and the deflecting distance after passing through the electric field

The force that accelerates the ion in the perpendicular direction to the incident direction is,

$$F = m\frac{dv}{dt} \approx m\frac{\Delta v}{\Delta t} = m\frac{v_h}{t_1} \qquad (2.26)$$

where v_h is the final velocity of the ion in the perpendicular direction when the ion just exits from the electric field, and

$$\tan(\alpha) = \frac{y_2}{x} = \frac{(y_2/t_2)}{(x/t_2)} = \frac{v_h}{v_0}\ . \qquad (2.77)$$

From equation (2.73) and equation (2.76), there is a relation

$$\frac{y_2}{x} = \frac{Ft}{mv_0} = \frac{Fb}{mv_0^2}. \qquad (2.78)$$

Substituting equation (2.71) for F in equation (2.78) gives

$$\frac{y_2}{x} = \frac{(eU/d)b}{mv_0^2} = \frac{eUb}{mv_0^2 d} = \frac{[(1/2)eUb]}{[(1/2)mv_0^2 d]} = \frac{eUb}{2E_0 d},$$

or

$$y_2 = \frac{eUbx}{2E_0 d}. \tag{2.79}$$

The total deflecting distance y_0 from the center of the primary ion beam before passing the field is the sum of equations (2.75) and (2.79):

$$y_0 = y_1 + y_2 = \frac{1}{4}\frac{eUb^2}{E_0 d} + \frac{1}{2}\frac{eUbx}{E_0 d}$$

or

$$y_0 = \frac{1}{2}\frac{eUb}{E_0 d}\left(\frac{b}{2} + x\right). \tag{2.80}$$

It is seen that the total beam bending distance depends on the electrostatic field voltage U and the original ion energy E_0, while others are constants. By adjusting U and measuring y_0, we are able to know the ion energy E_0, that is

$$E_0 = \frac{1}{2}\frac{eUb}{y_0 d}\left(\frac{b}{2} + x\right). \tag{2.81}$$

The measurement error of E_0 can be estimated by:

$$\frac{dE_0}{dy_0} = E_0^{'}(y_0) \Rightarrow approx. \frac{\Delta E_0}{\Delta y_0} = E_0^{'}(y_0),$$

or

$$\Delta E_0 = E_0^{'}(y_0)\Delta y_0,$$

that is,

$$\left|\Delta E_0\right| = \frac{1}{2}\frac{eUb}{d}\left(\frac{b}{2} + x\right)(y_0)^{-2}\Delta y_0. \tag{2.82}$$

2.7 Measurement of beam current (Yu Zengliang, 2006)(Yu Liangdeng, 1997)

Measurement of the ion beam current can be done both electrically and thermally (Yu Zengliang, 2006). In my research an electric mode was used for measurement of ion beam current. The ion beam current measurement is essential for ion implantation since it is the parameter related to fluence for determining time of implanting the sample.

The electrical method measures total ion charge delivered and then converts this to a beam current. Figure 2.9 schematically shows components of the ion beam current measurement device, a Faraday cup. The first plate (top) is a grounded electrode (aperture) for preventing ions from hitting the electron suppressor plate. The second plate is the electron suppressor which is given negative voltage at -100 - -500 V. When ions bombard the measurement piece of the Faraday cup at the bottom, secondary electrons will be emitted from the piece surface. The surface loses the negative charges of the electrons or in other word it gains positive charges which will be sent to the measurement meter and consequently the measured current will be higher than it should be. To prevent the error, the emitted secondary electrons must be suppressed and collected back to the measurement piece of the Faraday cup. The third is an electron collector which is normally a conducting tube and connected to the measurement piece to collect secondary electrons and send them to a current meter (Ammeter). The three components are insulated each other. An empirical rule tells that the length of the tube and the diameter of the measurement piece or the Faraday cup should be in a ratio of 3:1.

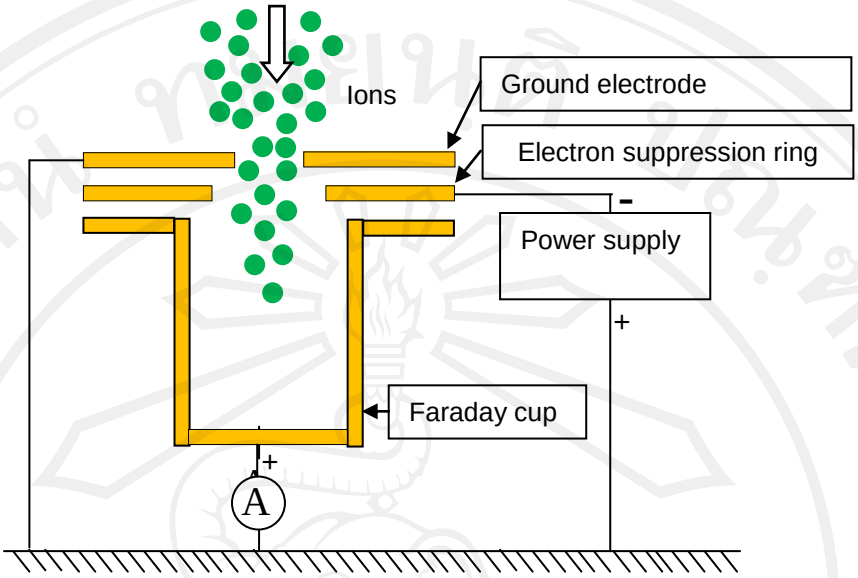

Figure 2.9. Schematic diagram of measurement of ion beam current using the Faraday cup (Yu Zengliang, 2006).

2.8 Fundamentals of ion implantation

2.8.1 Interaction of energetic ions with solid surface

When a primary ion bombards a solid target surface and penetrates inside the solid, various physical processes occur, as shown in Figure 2.10. At the top surface of the solid, due to the collision between the ion and the atom of the target, some electrons in the target may be emitted from the surface, which is called secondary electron emission. The secondary electron emission will be described later since the process has importance in accuracy measurement of ion beam current. The elastic collision between the ion and the target atom may cause the incident ion to be back-scattered. When the ions impact with the target atom, electrons of the atom may be excited and then fall to the lower energy level to produce X-ray, visible light, UV, or

photon emission. When ions penetrate in the solid, its energy, momentum, and charge are transferred to the target atoms. If the collision energy is larger than the critical energy for displacement of the solid atom, the solid atom is displaced. A series of consecutive collisions and displacements occur in the solid to form a collision cascade. A consequence of the collision cascade is damage to the target material structure, creating vacancies, interstitials, etc. When an ion loses energy continuously until finally stops below the surface, it is an implanted ion.

Electrons emitted from a solid surface that is bombarded with energetic incident ions are called secondary electrons, and the phenomenon is called secondary electron emission (Yu Zengliang, 2006). The parameter characterizing secondary electron emission in any given situation is the secondary electron emission coefficient. This is defined as the mean number of secondary electrons produced by each incident ion. The secondary electron emission coefficient depends on the incident ion energy, charge state of the incident ion, target material, and a rough or convoluted surface. Biological organisms have structurally complex surfaces and are electrically inert as well. Therefore, the secondary electron emission coefficient from the biological organism surface is greater than that from metallic or semiconductor surfaces when they are ion-bombarded under similar implantation conditions (Yu Zengliang, 2006).

2.8.2 Stopping cross section

Ion energy loss during ion penetration can be described by the stopping cross section $S(E)$, which is defined by

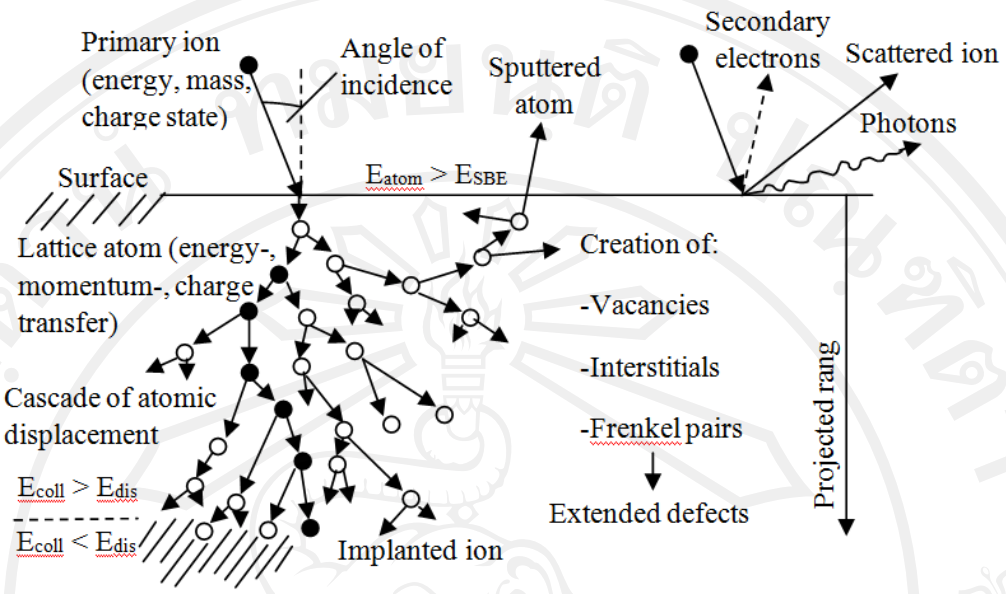

Figure 2.10. Schematic drawing of ion and solid interaction (Yu Liangdeng, 1997).

$$S(E) = -\frac{1}{N}\frac{dE}{dx}, \tag{2.83}$$

where dE is the energy loss of the ion travelling a distance dx and N is the number density of the target atoms.

For a two element target with compositions of $A_m B_n$, the mean stopping cross section is given by

$$S^{A_m B_n} = mS^A + nS^B \quad \text{(mean } S \text{ per molecule, for compounds),} \tag{2.84}$$

$$S^{A_m B_n} = \frac{m}{m+n}S^A + \frac{n}{m+n}S^B \quad \text{(mean } S \text{ per atom, for mixtures).} \tag{2.85}$$

2.8.3 Ion implantation range and projected range

The stopping cross section is the most fundamental and important concept in the ion solid interaction, which can lead to calculation of the projected range of ions.

The total path length R of the implanted ion in a solid is calculated by

$$R = \int_0^{E_0} \frac{1}{N} \frac{dE}{S(E)}, \tag{2.86}$$

where E_0 is the original energy of the incident ion. The shortest distance from the top surface of solid to the depth where ions stop is called the projected range R_p, as illustrated in Figure 2.11, which is defined by

$$R_p = R\cos\phi, \tag{2.87}$$

where ϕ is the deviating angle of the incident ion from the normal. An approximation for the relationship between the total path length and the projected range is

$$\frac{\overline{R}}{\overline{R}_p} \approx 1 + \frac{1}{3}\frac{M_2}{M_1}, \tag{2.88}$$

where $\overline{R}$ is the average ion path length, $\overline{R}_p$ is the average ion projected range, M_1 and M_2 are the masses of the ion and the target atom, respectively. This is a fairly good approximation for the case of low energies.

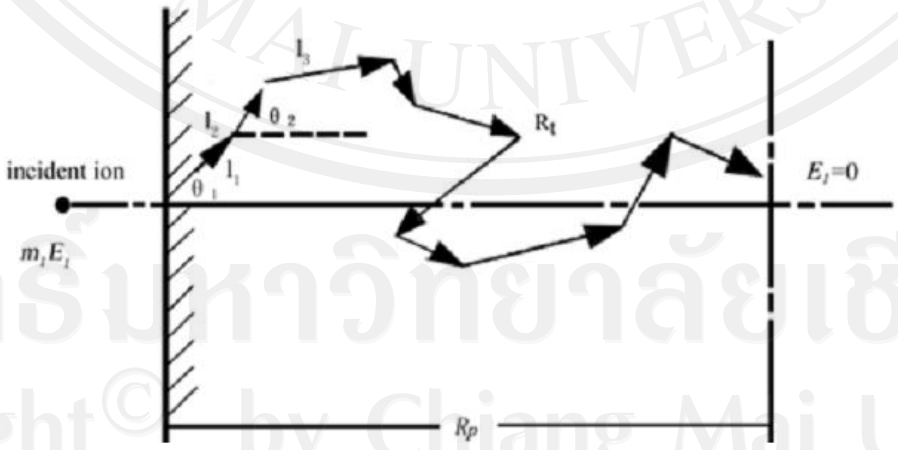

Figure 2.11. Schematic of ion's total path length and projected range (Yu Zengliang, 2006).

2.9 Interaction between energetic ions with DNA

2.9.1 DNA structures

A DNA molecule is composed of two poly-deoxyribonucleotide stands. The backbone of each strand is made from a connection between phosphodiester and two nucleoside furan β-D-deoxyriboses via 3' and 5' bonds. Both strands are dextrogyrate. They wind in opposite direction around the same axis, forming a dextrogyrate double helical structure. The helix rise per base pair is 3.4 Å. Every ten nucleotides from a helical turn and the height of each turn is 34 Å. The bases are inside the helix with their planes perpendicular to the helical axis. Phosphates are outside. The average diameter of the helix is 20 Å. The two strands are linked by hydrogen bonds between base pairs. The model of DNA is shown in Figure 2.12.

The spatial arrangement of base pairs is remarkably specific. Each adenine residue is paired with a thymine residue $(A = T)$ by two hydrogen bonds, and each guanine residue is paired with a cytosine residue $(G \equiv C)$ by three hydrogen bonds. Since the bases from two strands are on the same plane, they must be adapted to the phospho-deoxyribose backbone. Thus a base pair must be composed of a purine and a pyrimidine, and at positions opposite to pyrimidine must be purine. However, note that adenine (A) and cytosine (C) cannot form a base pair, neither can guanine (G) and thymine (T) form a hydrogen-bonded pair. This means that on the position opposite to A must be T and on the position opposite to G must be C.

The total number of the purine bases in a DNA molecule is the same as the number of pyrimudine bases. This is determined by the strict pairing rule between two

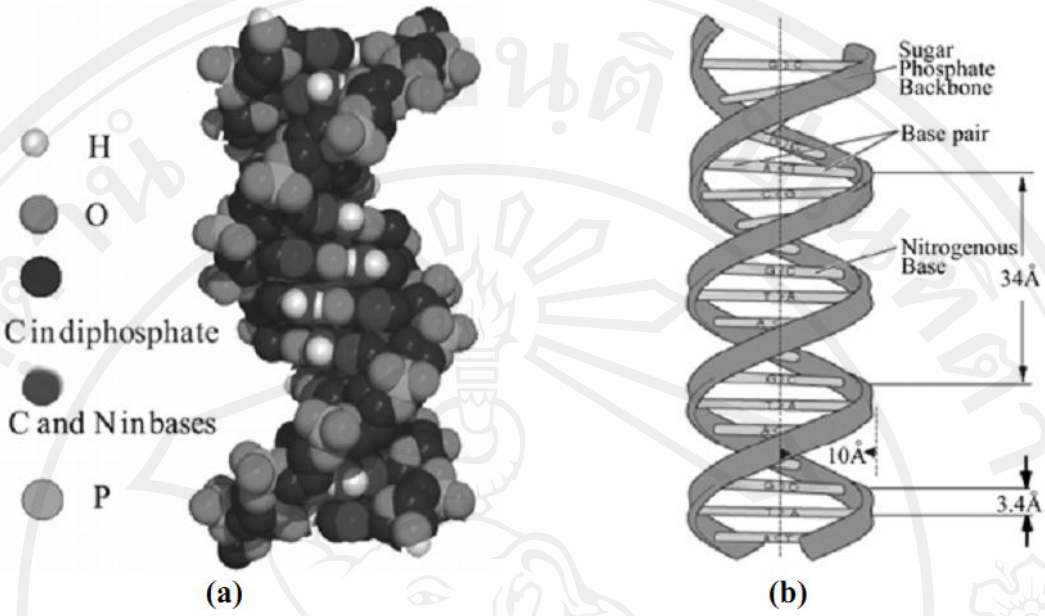

Figure 2.12. Schematic diagram of DNA. (a) The model of DNA double helix and (b) the scheme of the marcromolecule.

single strands in the DNA molecule. But on each strand the bases types in front and behind are not controlled by any rule. Hence in a DNA molecule containing a large number of bases, information that can be carried is extremely large. However, the versatile structure is maintained in the replication process only if the DNA molecule suffers no damage.

2.9.2 Fluence

The ion implantation fluence is an important parameter determining physical and chemical changes of materials including biological living materials. It should be noted that the fluence used here is different from the concept of dose used in radiobiology (Yu Zengliang, 2006). Fluence is defined as the number of incident

particles passing through unit cross sectional differential area. The conventional unit of fluence is ions/cm^2. The fluence can be estimated by

$$Fluence = \frac{It}{eA}, \tag{2.89}$$

where I is the target current in ampere,

t is the total implantation time in second,

e is magnitude of charge on electron (1.6022 x 10^{-19} C),

A is the implantation surface area in cm^2 .

2.9.3 Breaks of DNA single strands and double strands

Helical strands are the basic structure of all regular linear polymers in nature. This spatial configuration provides every individual with the same spatial orientation in its molecules, namely every individual forms the same secondary bond. Otherwise, if some secondary bond in the structure were stronger than others, instability would occur. At first glance, a DNA molecule is a fairly irregular polymeric strand and seemingly thus cannot form regular helical strands. But most DNA molecules contain two complementarily structural polynucleotide strands. The helical structure is stabilized by secondary internal and external bonds. Two strands are bonded by hydrogen bonds produced from complementary purine and pyrimidine base pairs. This arrangement stacks their flat planes on each other. A strand alone cannot form a regular backbone. Because pyrimidine is smaller than purine, the angle of helical spatial orientation would change with base sequence. This is obviously not a proper arrangement. As every base pair (-purine-pyrimidine) is the same in size, the double helical DNA formed from the complementary base pairs can have a regular structure and thus is also the most stable structure.

Double helical DNA molecules are quite stable at physiological temperatures. To disintegrate a DNA molecule, the hydrogen bonds between the double helical strands must be broken. But this is not to say that the DNA double helical structure is a totally fixed strong structure. In some cases, such as being impacted by energetic ions, DNA molecules and atoms can be displaced and rearranged to cause breaking of the double helical DNA single strand and double strands, despiralization and cross-linking.

2.9.4 Gel electrophoresis

Gel electrophoresis is a method used to separate proteins by charge and/or size. The total charge of DNA is negative since phosphate groups in the DNA backbone carry negatively charged oxygen molecules giving the phosphate sugar backbone of DNA an overall negative charge. Figure 2.13 shows a schematic diagram of the gel electrophoresis.

Ion-bombarded DNA is analyzed using gel electrophoresis for topological form change of DNA. A double-strand DNA is originally in the supercoiled form. When DNA has a single strand break, it would be in a relaxed form, and when DNA has a double strand break, it would be in a linear form. In gel electrophoresis, different DNA forms move in an electrical potential in different speeds, the linear form the fastest, the supercoiled form the second, and the relaxed form the slowest, due to different resistances from the gel. After a certain time period of running, different DNA forms are separated in the gel and the separations are used to identify the DNA forms. To observe movement of the DNAs, ethidium bromide is used to stain the DNAs. Stained DNAs can be visualized under ultraviolet (UV) light.

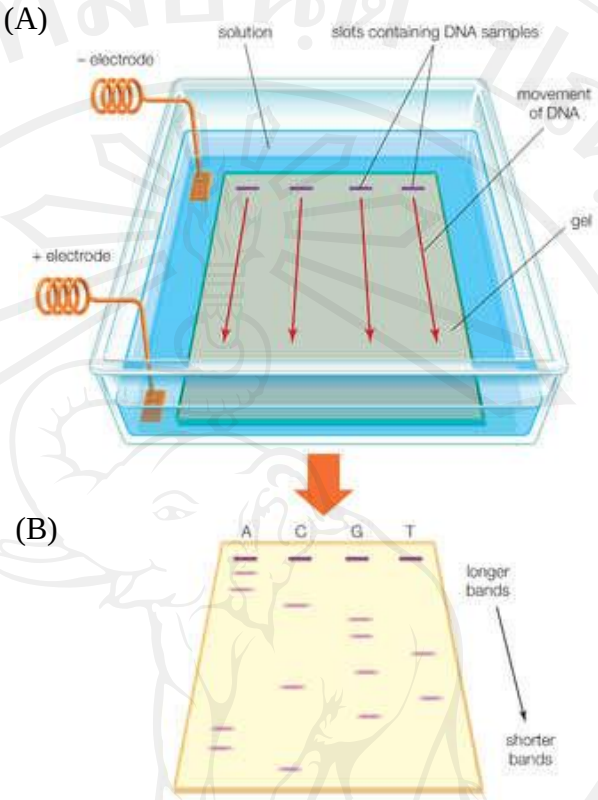

Figure 2.13. Schematic diagram of gel electrophoresis. (A) Equipment for gel electrophoresis method. An electric field pulls DNA in different forms (relaxed, supercoiled and linear forms) to pass agarose gel from the cathode pole to the anode pole as the total charge of DNA is negative. (B) Result of electrophoresis showing mobility of different DNA forms.